Preparation of CoNi high surface area porous foams by substrate controlled electrodeposition†

Lidija D. Rafailović,*[a,b] Christoph Gammer,[b] Christian Rentenberger,[b] Christoph Kleber,[a] Adam H. Whitehead,[a] Bernhard Gollas,[a,c] and Hans-Peter Karnthaler[b]

Please cite as

L. D. Rafailovic, C. Gammer, C. Rentenberger, C. Kleber, A. H. Whitehead, B. Gollas, H. P. Karnthaler.

Phys. Chem. Chem. Phys., 14, 972-980 (2012).

DOI:10.1039/c1cp22503k

We demonstrate that nanofabrication of 3D dendritic CoNi alloy foams with an open porous structure can be achieved by electrodeposition onto a single-crystalline Cu (111) substrate at ambient conditions. The very low wettability of this substrate caused by its low surface energy allows tailoring the CoNi deposit morphology. This is concluded from a comparison of polycrystalline Cu substrates with single-crystalline ones of different orientations. The advantages of the present CoNi alloy foams are low internal stresses and good mechanical stability on the substrate. In a second step, by comparing the catalytic properties of the achieved foam with those of CoNi layers obtained on polycrystalline Cu substrates, it is shown that the morphology of the CoNi layers has a decisive influence on the kinetics of the surface redox reaction. The higher reaction rate makes the open foam suitable as catalyst for oxygen evolution in electrolysers. The reversibility of the redox process provides a great potential for the achieved porous layers to be used as positive material in alkaline batteries.

1 Introduction

Electrodeposition is regarded as a viable process for nanofabrication [1] and - even though it has received considerable attention from both theoretical and experimental side - the production of tailored nanosized structural features especially for alloys has still to be closer investigated. Recently, attention has been paid to make dendritic nanomaterials by electrochemical procedures. [2–4] Also, pattern formation and its spontaneous evolution in non-equilibrium conditions systems through electrochemically grown silver dendrites within a template free deposition was reported as a way to large scale synthesis of multiplied twinned Ag nanowires. [5] On the other hand, dendritic structures formed by electrodeposition on the surface of chosen substrates can yield a high surface area which is advantageous in certain electrochemical devices (e.g. fuel cells, sensors and batteries). An open structure is crucial for high rates of mass transport, that is generally important for catalysts and electrodes for electrochemical devices. [6,7] A technique based on hydrogen co-evolution during electrochemical deposition of metals (Cu, Sn) and their alloys was used to produce open dendritic structures. Hydrogen bubbles seem to be important as a dynamic negative template; the resulting structures are foams with porous walls. [8]

It is an aim of this work to investigate the influence of the substrate and that of hydrogen bubble detachment on the formation of dendritic foam structures. Therefore, at first instance, two different substrates, polycrystalline (PC) Cu and single-crystalline (SC) Cu (111) and (123) were used. Special attention was devoted to the phenomenon of wetting. The increasing interest in the construction and application of surfaces with switchable liquid-solid adhesion for various practical purposes in smart and fluid-controllable devices, mainly tailored by surface morphology emphasizes the importance of fundamental research in this field. [9] The wettability plays an important role in electrodeposition, that can be even used as a novel approach for selective growth of porous hierarchical structures in the superhydrophilic region. [10] Therefore the surface wettability governed by microstructure and interfacial energy was investigated and compared for both substrates to give insight into the nature of solid-liquid-gas interactions during electrolysis in aqueous solutions.

One of the greatest challenges in the forthcoming years undoubtedly will be energy storage; here nanostructured materials become increasingly important due to their unique properties. [11] Electrodeposition with high applied overpotential during metal plating represents an excellent approach to achieve hierarchical structures with nanometre size domains. In recent years, Co compounds have been used as positive electrode materials to improve electrochemical performance. [12] As

[0a] *CEST, Centre of Electrochemical Surface Technology, Viktor-Kaplan-Strasse 2, 2700 Wr. Neustadt, Austria. Fax: +43 2622 22266-50; Tel: +43 2622 22266-46; E-mail: lidija.rafailovic@cest.at*

[0b] *University of Vienna, Physics of Nanostructured Materials, Boltzmanngasse 5, 1090 Vienna, Austria.*

[0c] *Graz University of Technology, Institute for Chemistry and Technology of Materials, Stemayergasse 16, 8010 Graz, Austria*

charge/discharge processes in general are limited by the reaction kinetics, the search for a device that can deliver high power is an active field.[13] Therefore, the preparation of materials with a high surface area can improve device performances because more material is available on the surface for charge compensation as well as for energy storage.[13]

2 Methods

Electrodeposition was conducted in the galvanostatic regime at a current density of 0.1 A cm^{-2} at room temperature without stirring, using the potentiostat IMP 83 PC-10, (Jaissle, D). A simple bath without any organic additives in a solution containing: 0.025 M $NiSO_4$+0.1 M $CoSO_4$; 0.5 M NH_4Cl and 3.5 M NH_4OH (Sigma-Aldrich) at pH=10. As an anode we used a Ti plate covered with RuO_2/IrO_2 (10 cm^2 geometric area), placed parallel at the distance of 2 cm to the substrate.

Different Cu substrates were used as cathodes: Polycrystalline Cu and single-crystalline Cu with two different crystallographic orientations. The polycrystalline Cu substrate was cut out from Cu rods electrolytically prepared. The surface preparation of the polycrystalline Cu substrates prior to deposition included polishing with SiC emery paper (1200), washing and treating in an ultrasonic bath, etching quickly in concentrated HCl (a few seconds) and cleaned with distilled water and dried in a stream of compressed nitrogen. The single-crystalline substrates were prepared from a Cu single crystal of high purity (5N) grown by a modified Bridgman technique. The single crystal was cyclically annealed and furnace cooled to minimize the density of the grown-in defects ($<5 \cdot 10^5$ cm^{-2}).[14] The single crystal was oriented by the X-ray Laue method and cut in two different orientations: near to (111) and in addition in an orientation near the middle of the orientation triangle (near (123)). The surface treatment of the single-crystalline substrates included polishing with SiC emery paper (1200), washing and treating in an ultrasonic bath; additionally in one case a final electropolishing step was carried out in a solution of a mixture consisting of H_3PO_4 and CH_3OH/C_2H_5OH at room temperature.

Cyclic voltammograms were obtained in a three electrode cell using the potentiostat VoltaLab 40, PGZ 301 (Radiometer Analytical, F). The working electrodes were prepared from the polycrystalline and single crystalline (111) Cu substrates and had a diameter of 3 mm. The counter electrode was a Pt mesh with a large surfaces area much larger than that of the working electrode and a silver chloride electrode (Ag/AgCl) was used as a reference electrode. A scan rate of 50 mV s^{-1} was applied.

To characterise the different substrates, a contact angle technique was used to quantitatively measure the wetting of the materials. Contact angle measurements were carried out by applying droplets of 10 μl of distilled water to 1 cm^2 of the PC and SC substrate surfaces. In our case distilled water is considered as a good reference because the electrolyte used for electrodeposition is relatively simple and contains no organic surfactant often added to reduce surface tension. Distilled water was also used to avoid the enhanced oxidation of Cu, that would occur by the alkaline electrolyte in contact with air. The contact angle was measured using an instrument equipped with a CCD camera (Krüss, DSA10); the mean values are given as an average of 5 measurements.

The surface roughness measurement was performed on an evaluation length of 1.75 mm on bare substrates using the computer controlled device Perthometer S2, Mahr (D); each measurement was repeated three times.

The phase content and the crystallite size were determined by XRD[15] using a X'Pert Powder diffractometer from PANalytical, (CuKα 40 kV/ 30 mA) in Bragg-Brentano geometry. The measurements were performed in step-scan mode over the range 2θ=20–110° with a step size of 0.05° and a counting time of 10 s/step. Evaluation of the phase volume and crystallite size was done by Rietveld refinement[16] using the TOPAS software (Bruker AXS, D). The stress determination[17] were done on the same device using an automatic Eulerian cradle. The area of the sample irradiated by the X-ray beam was in the range of several mm^2. Lattice spacing (d) measurements were performed for the stress detection on the lattice planes: (100), (002), (101) of the hexagonal Co phase. This procedure was repeated for each sample at three different azimuthal positions (due to the assumed radial stress symmetry a mean value of d was taken) and at six different tilt angles (ψ). For each sample orientation a corresponding strain value $\varepsilon(\psi) = (d - d_0)/d_0$ was calculated. In this relation d_0 refers to the lattice spacing of the stress-free reference sample (electrodeposited hexagonal close-packed $Co_{90}Ni_{10}$ powder embedded in epoxy resin). The residual stress in the samples was then calculated by means of linear regression in an $\varepsilon(\psi)$ versus $\sin^2\ \psi$ diagram using the modified equation describing a stress state with cylindrical symmetry (σ_{22}=σ_{11}):

$$\varepsilon(\psi) = \frac{1+\nu}{E}(\sigma_{11} - \sigma_{33})sin^2(\psi) + \frac{1}{E}(\sigma_{33} - 2\nu\sigma_{11})$$

whereby σ_{11} and σ_{33} refers to the stress component parallel and normal to the layer surface, E denotes the corresponding Young's modulus (stiffness), and ν refers to the Poisson's ratio of the material.[18,19] The surface morphology of the obtained deposits was analysed with a scanning electron microscope (SEM) with a field emission gun (XL 30 ESEM-FEG, FEI).

3 Results and discussions

3.1 Wettability of the Cu substrates

3.1.1 Single-crystalline and polycrystalline Cu substrates

The wetting of a solid with water in gas as a surrounding medium is dependent on the three interfacial energies: solid-gas γ_{SG}, solid-liquid γ_{SL} and liquid-gas γ_{LG}. According to Young equation the ratio between them determines the contact angle.[20]

$$\gamma_{SG} = \gamma_{SL} + \gamma_{LG} \cos\theta_{CA}$$

A contact angle (θ_{CA}) less than 90° for water indicates hydrophilic and higher than 90° hydrophobic surfaces. Fig. 1a shows the measurement of θ_{CA} for the PC substrate yielding θ_{CA}=68.5°± 1.2°. The value for the electropolished SC(111) substrate is considerable higher θ_{CA}=89°± 1.5° (Fig. 1b).

3.1.2 Influence of the surface roughness

To study if the roughness has an effect on the wettability, the electropolished SC(111) substrate was compared with a mechanically polished SC(111) substrate (mean roughness of 0.023 and 0.25μm, respectively). The surface roughness of the polished SC is comparable to that of the polished PC. The polished SC(111) showed a high contact angle θ_{CA}=95°± 1.5° (Fig. 1d) similar to that of the electropolished SC(111) (Fig. 1b). In the case of the PC substrate the application of different preparation methods yielded that they did not have a significant effect on θ_{CA}.

3.1.3 Influence of the surface orientation

An investigation of the influence of the crystallographic orientation of the surface on the wettability was carried out on single-crystalline substrates with similar roughness but two different orientations: firstly, an orientation of low surface energy near (111) and secondly, an orientation with high surface energy near the middle of the orientation triangle about (123). Fig. 1c shows that in the case of the (123) orientation θ_{CA} was considerably reduced as compared to that of the (111) orientation (73°± 1.1° and 95°± 1.5°, respectively).

This result shows that the wettability is strongly influenced by the crystallographic orientation of the surface. In contrast the surface roughness has a minor influence as shown in section 3.1.2. The contact angle of the PC substrate is lower since the randomly oriented grains have for statistical reasons predominantly orientations in the middle of the orientation triangle and only in rare cases orientations of low index planes with low surface energies. This is supported by the results by Hasouna et.al.[20] reporting that in a strongly textured polycrystalline Cu having grains with their surfaces predominantly oriented parallel (111) the contact angle increases.

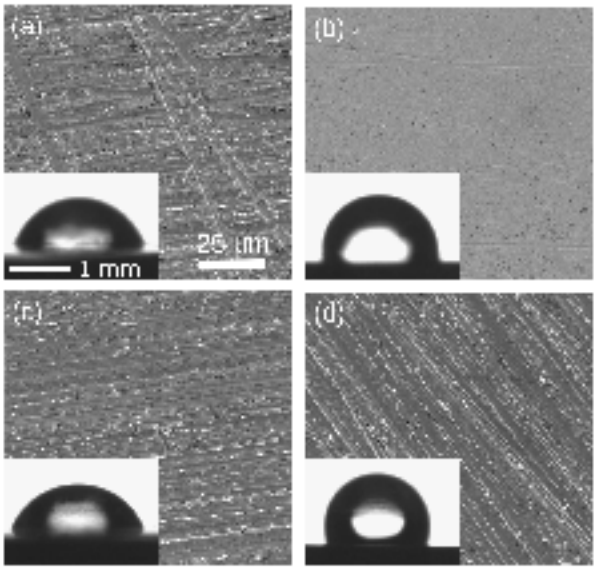

Figure 1 Wettability of the Cu substrates; droplets of distilled water used to measure the contact angle and SEM images of the corresponding surfaces. (a) mechanically polished polycrystalline substrate, (b) electropolished single-crystalline (111) substrate, (c) mechanically polished single-crystalline (123) substrate and (d) mechanically polished single-crystalline (111) substrate.

3.2 Morphology of the CoNi deposits

3.2.1 Influence of the crystallographic orientation of the surface as deduced from single-crystalline substrates

Fig. 2 shows comparison between CoNi deposits on surfaces oriented parallel to an orientation in the middle of the orientation triangle near (123) and near (111), respectively. Electrodeposition was done under the same conditions (0.1 A cm^{-2} for 39 min). A nonporous structure with a presence of just of a few shallow craters was formed on the SC(123) substrate (Fig. 2a). In contrast, deposition on the SC(111) substrate yields a very pronounced open, three-dimensional porous structure (Fig. 2b). Therefore, the achievement of the open foam structure can be assigned to the surface orientation of the SC(111) substrate. The influence of the crystallographic orientation of the surface is interpreted as follows: A surface oriented near (123) (in the middle of the orientation triangle, i.e. away from the low energy orientation) has a structure with a high density steps and facets of low energy planes. In contrast, a surface ori-

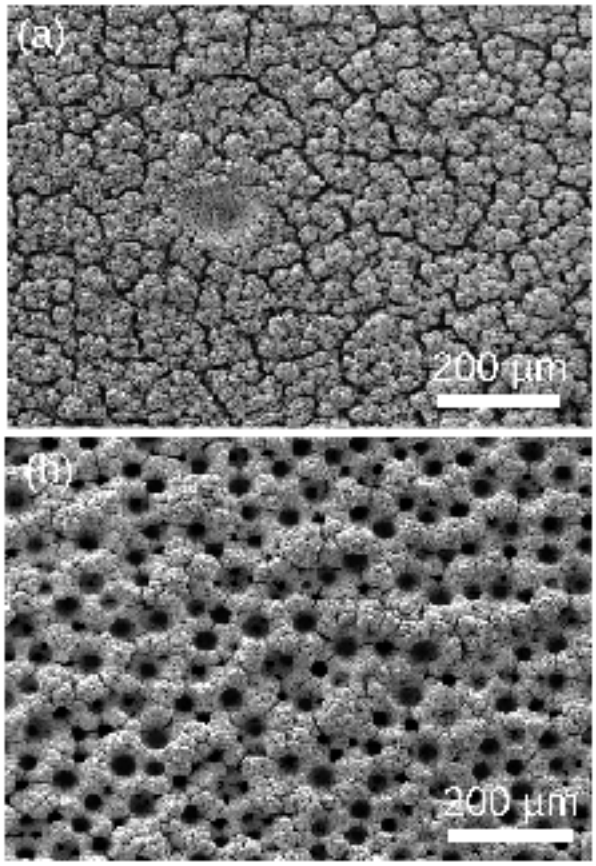

Figure 2 SEM micrographs of the $Co_{80}Ni_{20}$ deposits (top view) on mechanically polished single-crystalline Cu substrates with different crystallographic orientation of the surface; (a) orientation of the substrate near (123) leading to a dense deposit with a few shallow craters, (b) substrate orientation (111) leading to an open porous CoNi deposit structure.

entated near (111) is formed by large segment of (111) planes and has much lower density of steps and facets as compared to a surface near (123) (in the face-centred cubic structure the (111) planes are the most densely packed having the the lowest surface energy corresponding to the deepest cusp in the Wulf plot of the energy).[21] It is proposed that the steps and facets present on the surface can act as nucleation sites for the electrodeposition. Therefore the high nucleation density of a surface near (123) leads to a formation of homogenous fine-grained deposit (Fig. 2a). In contrast, the low energy of nucleation sites on (111) gives rise to the open, foam structure (Fig. 2b).

3.2.2 Comparison of polycrystalline Cu and single-crystalline Cu (111) substrates

Fig. 3 shows the CoNi deposits on PC and SC(111) substrates using a same current density of 0.1 A cm^{-2} like through this study. Fig. 3a is a SEM image (top view) of CoNi deposited on PC showing platelet structures with sizes from 1 to 3 μm. composed of nanograined crystallites are obtained. Fig. 3b shows a SEM cross section image of the 30 μm thick CoNi deposit. The deposit is rather dense, it contains some voids and a crack (C) at the interface between the substrate (S) and deposit (D). At larger scale the surface is smooth without large craters (Fig. 3c). It is of interest to point out that the structure of the deposit on the PC substrate (Fig. 3c) corresponds to the structure observed on the SC substrate with (123) orientation (Fig. 2a). This corresponds with a results of the wetting behaviour where the measured contact angles on PC and SC(123) are about the same. Therefore the same explanation is put forward based on the fact that the surface orientation of the various grains of the PC substrate have predominantly orientations within the orientation triangle and rarely low energy orientations as (111).

Fig. 3d, e and f show SEM micrographs of CoNi electrodeposited foams on a SC(111) substrate. The deposit shows a platelet structure as in the case of CoNi electrodeposited on the PC substrate, but with a finer morphology (compare Fig. 3a and d). Applying the same experimental conditions as in the case of deposition on the PC substrate, the deposits formed on the SC substrate consist of approximately 10 times smaller platelets (length of 0.1-0.5 μm) that are elongated in this case.

A comparison of the thickness of the deposits yields a value of around 30 μm in the case of the deposit on the PC substrate. The thickness of the deposit on the SC substrate is larger (45 μm), because approximately the same amount of material (as deduced from the current efficiency measurements) in the case of deposit on SC substrate yields a larger thickness of a porous structure.

It is found that on the SC(111) substrate an open foam structure can be achieved on the whole electrode surface. The deposit consist of dendrites made up by platelets containing very fine grains (Table 1).

3.2.3 Influence of the surface roughness

To study the influence of the surface roughness, CoNi deposits obtained on substrates with different surface preparations were compared. Fig. 2b shows a deposit obtained on a mechanically polished SC(111) substrate. The comparison with the deposit obtained on the electropolished SC(111) substrate (Fig. 3f) shows that an open porous structure is obtained in both cases. Similar studies were performed in the case of the PC substrate

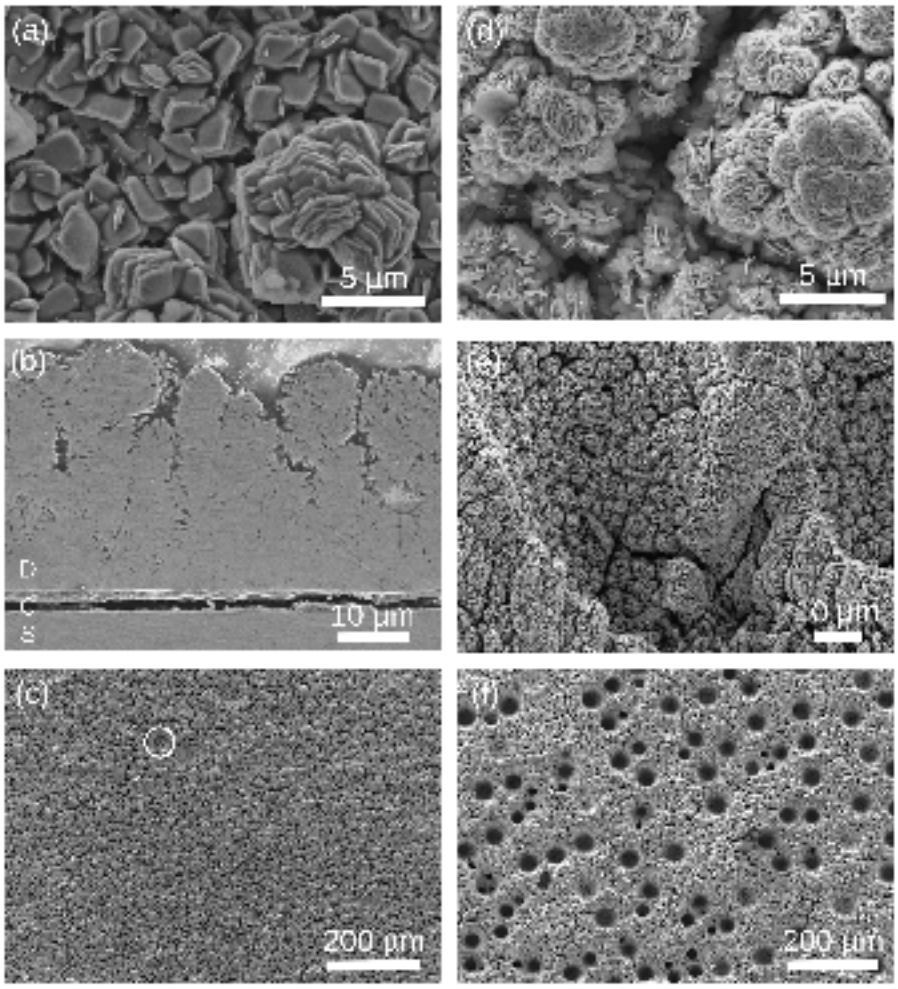

Figure 3 SEM micrographs of CoNi electrodeposits on polycrystalline Cu substrates ((a)-(c)) and single crystalline (111) Cu substrate ((d)-(f)) after the same deposition time (t=39 min). (a) top view of the deposit showing platelets (1-3 μm). (b) cross-section of (a), substrate (S), crack (C) between S and the deposit (D) are marked. (c) dense CoNi deposit with just a few craters (one marked in the image). (d) top view showing an open dendritic structure dominated by big dendrites (about 20 μm apart) that are formed of small elongated platelets (0.1-0.5μm). (e) side view of the 3D dendritic foam structure of CoNi deposit. (f) top view of the open dendritic structure.

Substrate, thickness of deposit	Relative phase content [wt.%] HCP	FCC	CoNi average crystallite size [nm]	CoNi macrostresses σ_{11} [GPa]	σ_{33} [GPa]
polycrystalline Cu, 30 μm	93	7	14	-1.85	-0.89
single-crystalline Cu (111), 45 μm	80	20	9	0.74	0.43

Table 1 CoNi electrodeposits on different Cu substrates. Results of the XRD measurements: content of HCP and FCC nanograins in solid solution of CoNi; for the Co (HCP) nanograins grain size and values of the internal stresses are given (compressive stresses are indicated by a negative sign, tensile stresses are positive).

yielding the result that the surface treatment does not have a pronounced effect on the morphology of the deposit.

3.3 Microstructure of the CoNi deposits

CoNi forms a solid solution over the whole range of compositions. At low Ni contents ($<$ 25 at.%) the hexagonal closed packed (HCP) phase is formed whereas at higher Ni contents the face-centred cubic (FCC) phase is the equilibrium phase. Fig. 4 shows X-ray patterns of CoNi deposited both on a SC(111) and a PC Cu substrate using the same deposition conditions. Peaks corresponding to the HCP phase (marked by $*$) are dominating. In addition to the HCP phase, some peaks corresponding to the FCC phase (marked by x) are identified. In the XRD intensity profile on the SC substrate the CoNi the (111) Cu reflection of the SC substrate is present since the deposit is porous with a pronounced open structure (Fig. 3e). Some peaks are observed at higher 2θ angles (especially on PC) since the X-ray beam partially penetrates the deposited layer.

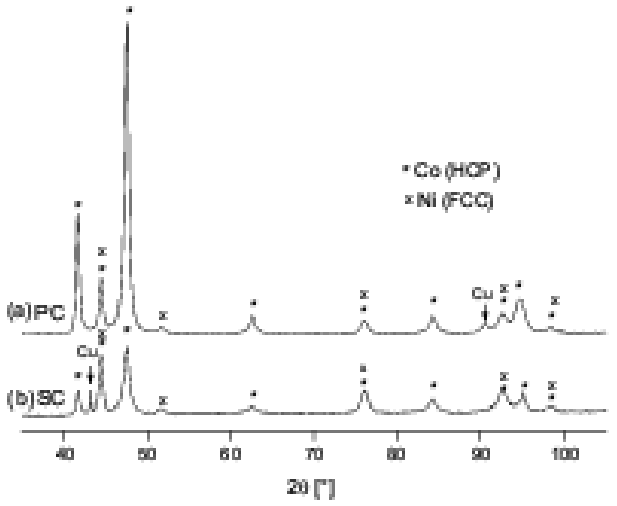

Figure 4 CoNi electrodeposits; the XRD patterns show the intensity (in arbitrary units) as a function of the scattering angle 2θ. (a) polycrystalline Cu substrate, (b) single-crystalline Cu (111) substrate.

In Table 1 the results of the X-ray measurements are summarized. Rietveld analysis using all peaks in the X-ray profile was performed to measure the crystallite size. For the deposit obtained on the PC substrate an average crystallite size of 14 nm was obtained for the HCP phase. Therefore the XRD measurements shows that the plate-shaped structures observed in the SEM (Fig. 3a) contain about 25000 crystallites in volume.

XRD analysis yields a Ni-rich FCC phase of 7 wt.% for the deposit on the PC substrate. At the beginning of the deposition a higher content of Co would be expected, as deduced from the polarization diagram due to the lower overpotential for Co deposition on a Cu substrate in comparison to Ni for the electrolyte used in this case.[22] This is not the case here, since at the beginning of the deposition process the growth rate of the Ni-rich FCC phase on the FCC Cu substrate is enhanced, as deduced from localised energy-dispersive X-ray spectroscopy of the cross-sectional sample (Fig. 3b and e). On further deposition, as expected, the lower overpotential for Co deposition in comparison to Ni increases the Co content in the deposit building up the HCP structured CoNi phase. The anomalous character of the co-deposition of Co^{2+} and Ni^{2+} ions from the solution, where the less noble element (Co) is deposited preferentially to the more noble (Ni), is characteristic for electrodeposition of iron group metals (Co, Ni, Fe),[23] and is enhanced in addition by the lower Ni^{2+} concentration in the electrolyte.

Rietveld analysis for the deposits on the SC(111) substrate yield an average crystallite size of 9 nm and thus a refinement as compared to CoNi with an average crystallite size of 14 nm deposited on the PC substrate (Table 1). Deposits on the SC(111) substrate show a higher percentage of the Ni-rich FCC phase (20%) as compared to those of the PC substrate (7%) (Table 1). This indicates that epitaxial growth that could occur on SC(111) substrate. Also, the open structure could increase the relative phase content of the FCC structure, since the XRD signal obtained from the near substrate layer passing the foam is increased. The epitaxial growth on Cu was additionally checked by using HCP Ti as a substrate and applying the same conditions: in this case only the HCP phase and no FCC phase has been observed. To prove the proposed epitaxial growth further investigations are needed based on the study of the cross-section samples prepared by focused ion beam and carried out in a high-resolution transmission electron microscopy with a corrected objective lens to reveal the positions of the atoms.

3.4 Internal stresses of the CoNi deposits

The deposits obtained on the PC substrate show a high compressive stress (Table 1) that leads to the formation of cracks at the interface (Fig. 3b). To determine the stress the anisotropy of the elastic parameters in the deposited crystals was taken into consideration in a first approach. The elastic stiffness constants in the crystallographic direction corresponding to the observed specific diffraction peak were used for the residual stress calculations. Such an assumption would fit to the Reuss model (which assumes a homogeneous stress).[24] However, the stress values calculated from the different diffraction maxima show a strong variation suggesting that the Voigt model[25] is more adequate as it assumes a homogenous strain. This behaviour is most likely caused by the specific grain-grain interaction properties of the material. For further determination of residual stress determinations isotropic elasticity constants[26] were applied.

The presence of compressive stress is in agreement with the

results obtained for conventional direct current plating of nickel electrodeposits.[27,28] The high compressive stress is expected for deposits obtained from additive-free electrolytes and for deposits with structural parameters different to the substrate. Impurities in the deposit can also significantly increase the internal stress. In electrodeposited Ni, impurities are typically limited to interstitial types, particularly hydrogen, which can exist in solid solution or in form of bubbles within the grains in the grain boundaries and triple junctions.[28–30] During the electrodeposition of the $Co_{90}Ni_{10}$ deposit, an intensive parallel hydrogen evolution reaction occurs. Therefore, it can be assumed that incorporation of hydrogen takes place resulting in an increase of internal stress.

The XRD measurements show that the internal stresses are lower for the CoNi deposits on the SC(111) substrate than for the deposits on the PC substrate (Table 1). In general, a decrease in grain size is accompanied by an increase of the internal stress[31] but in the present case the different mechanism of hydrogen incorporation leads to reduced stress even though the grain size is reduced (Table 1). In the case of the SC(111) substrate less hydrogen is incorporated into the open foam as compared to the deposition on the polycrystalline substrate. Furthermore, due to the open dendritic structure hydrogen formed by decomposition of hydrides can leave the deposit more quickly leading to the contraction of the lattice and thus to tensile stress[31]. Therefore, the open foam structure shows a reduction and even a change of the sign of the internal stress which improves the mechanical stability of the dendritic deposit and its adhesion to the substrate.

3.5 Formation of an open foam structure

3.5.1 SEM investigations of the porous deposit

Fig. 5 shows an investigations of the open foam structure achieved on the mechanically polished SC(111) Cu substrate. The SEM investigation with higher magnification reveals that the structure consists of circular depressions of about 30-50 μm that are partly interconnected by smaller holes surrounding them (Fig. 5a). Hydrogen bubble size determines pore size of the CoNi foam and the thickness of the layer. Larger and more pronounced pore size leads to the higher thickness of the porous CoNi layer to that formed on the electropolished SC(111) substrate. A cross-section sample was embedded in a resin and polished. The deposited foam shows a good mechanical stability and good adhesion to the substrate. The SEM image of the cross-section (Fig. 5b) reveals a very deep crater formed as a consequence of hydrogen bubble template deposition. The deposit consists of dendrites, yielding a network of finer pores.

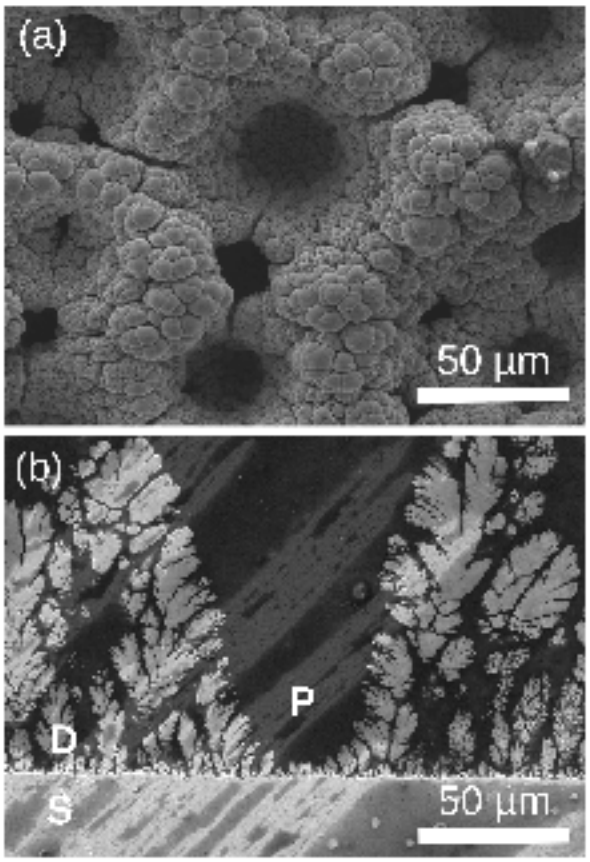

Figure 5 SEM images of the $Co_{80}Ni_{20}$ deposit obtained on mechanically polished SC(111) substrate (S). (a) top view of the open, porous CoNi foam showing a multimodal pore size distribution. (b) cross-section of a large pore (P) created by hydrogen templating. The deposit consists of dendrites (D) forming the foam structure.

3.5.2 Deposition under concurrent hydrogen evolution

The production of dendritic deposits can be achieved in the galvanostatic regime at a high current densities in additive-free aqueous electrolytes, leading simultaneously to significant hydrogen evolution as a parallel and competitive cathodic side reaction.[22] We have shown previously that the conditions necessary for the production of dendritic NiCo deposits on Cu PC substrates depend on the electrolyte composition and on the current density.[32] Production of dendritic deposits on PC substrates was enhanced by higher Co^{2+} concentration in the electrolyte and by increasing the current density.

Based on Faraday's law and weight measurements of the dried deposits, current efficiencies were calculated. In the case of deposition on the SC(111) and the PC substrate the current efficiency were comparable and less than 50% .Therefore, it can be concluded that the deposition process is not strongly influenced by the concurrent hydrogen evolution reaction per se, but rather by the hydrogen bubble formation and desorption.

3.5.3 Influence of the bubble desorption

A route for the production of open, porous metals (Cu, Ag)[8,33–35] with nanostructured walls[36] by hydrogen bubble templating during electrochemical process was recently introduced. Hydrogen evolution reaction, usually suppressed during electrochemical process, is on contrary promoted by electrodeposition conducted at high current density or overpotential.[37] Hydrogen bubbles formed by the electroreduction of H^+, serve as a dynamic template for a deposition of a self-supported 3D foam.[35] Hydrogen bubbles raised at different locations on the substrate during simultaneous growth within the metal, create pores in the layer after detaching from the the surface.[33]

In our approach, by appropriate choice of the substrate, in this case a SC(111) Cu substrate, an open, porous CoNi alloy foam structure is obtained at a significantly lower current density compared to that used to make a Cu[8] or Ag foam.[35] In our case the low wettability of the SC(111) substrate hinders the bubble desorption and promotes the formation of an open porous structure.

3.5.4 Schematic model for the formation of the porous structure

Fig. 6 presents a schematic drawing comparing the electrodeposition on the PC substrate (Fig. 6a) with that on the SC(111) substrate (Fig. 6b). Although the current efficiency was similar in both cases, implying the same rate of hydrogen evolution, the hydrogen bubble desorption is different.

In the case of the single-crystalline (111) substrate, in a first step a layer is formed with a deposition at the fewer surface steps acting as nuclei. The localized flow of the metal ions to the growing dendrites leads to the coalescence of hydrogen bubbles (Fig. 6c). This leads to the formation of larger hydrogen bubbles resulting in the outgrowth of an open foam structure (Fig. 2b, 3f). Larger hydrogen bubbles attached to the substrate result in very large and deep holes (Fig. 2b, 3f).

Furthermore, the hydrogen bubble desorption is affected by the surface energy and therefore depends on the substrate rather than on the kinetics of the hydrogen evolution reaction.[38] The SC(111) surface of low energy shows a reduced wettability compared to that of the polycrystalline surface. Therefore, the radius at which bubbles detach from the surface is larger in the case of single-crystalline substrate. The gas bubbles that stick to the substrate partly cover the substrate, templating the formation of holes in the deposited foam.

Locally, high local current densities, concentrated around bubbles due to their non-conductivity, causes faster growth of finer dendrites containing small platelets and fine crystallites. The microscopic current distribution is changed due to the adsorption of bubbles decreasing both conductivity and the effective electrode area.[37] As a final result, the current density distribution and coalescence of hydrogen bubbles create porous, foam-like, dendritic structures on different length scales (Fig. 5).

In the case of polycrystalline substrate, due to multiple nucleation sites, the deposit obtained shows no preferential hydrogen evolution sites. Thus a dense deposit is formed incorporating more hydrogen and containing only a small number of very shallow craters (Fig. 3c). Hydrogen evolution causes gas bubble stirring that changes the hydrodynamics and the mass transfer conditions in the near-electrode electrolyte layer.[37] This leads to the formation of a large amount of nuclei due to the numerous nucleation sites on the polycrystalline Cu substrate. These nuclei determine the following deposition process. The CoNi deposition is performed under conditions of slow diffusion of the cations from the solution to the cathode where a fast electroreduction occurs.

3.6 Enhanced catalytic ability of the open, dendritic structure

An investigation of the influence of microstructure and morphology on the catalytic activity was conducted on the different deposits. Fig. 7 shows cyclic voltammograms recorded in 0.1 M KOH at pH=12 on CoNi deposits of similar composition but different morphology, that were used to compare their catalytic activity. To provide a smooth reference sample to compare the influence of morphology the deposit obtained on PC was polished to about 500 nm thickness (Fig. 7a insert and curve (a)). Curves (b) and (c) corresponding to

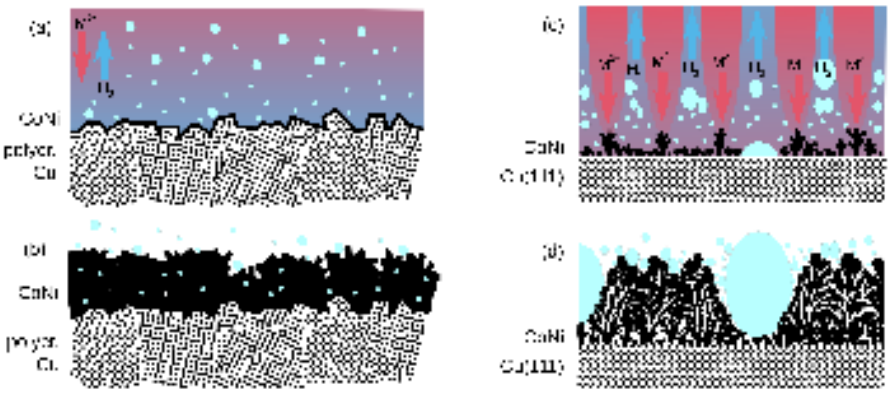

Figure 6 Schematic representation of the CoNi electrodeposition process during concurrent hydrogen evolution reaction. Flow of metal ions and hydrogen bubbles are indicated. (a) initial stage of electrodeposition on polycrystalline Cu dominated by the numerous nucleation sites of the surface of the substrate. The hydrogen bubble departure radius is rather small due to the high surface energy. (b) final stage of electrodeposition resulting in a dense CoNi deposit on polycrystalline Cu incorporating hydrogen. (c) initial stage of electrodeposition on single-crystalline (111) Cu substrate. The hydrogen bubble departure radius is much larger as bubbles stick to the surface. (d) formation of a dendritic foam structure as a consequence of hydrogen templating.

Fig. 7b and c show the results for the deposits on PC and SC(111) substrates, respectively. The peaks in the anodic region at 380 mV vs. Ag/AgCl for both deposits (on PC and SC(111) substrates) that precede the oxygen evolution reaction are attributed mainly to oxidation of the Co and Ni oxide/hydroxide compounds formed as a consequence of thermodynamically favourable reaction pathways where the Co and Ni oxide and/or hydroxide are formed. Namely, many redox couples of metal Co and Ni oxides and hydroxides can be found around this potential,i.e. for 1 e^- transfer at pH=12, electrode potentials for the reactions: $Co(OH)_3 + e^- \rightleftarrows Co(OH)_2 + OH^-$ and $3CoOOH + e^- \rightleftarrows Co_3O_4 + H_2O + OH^-$ or $NiO_2 + H_2O + e^- \rightleftarrows NiOOH + OH^-$ are E = 85 mV, 285 mV and 395 mV vs. Ag/AgCl, respectively. Therefore, the reactions observed here are attributed generally to oxidation and reduction of the Co and/or Ni between oxidation states II and IV. The cathodic peaks at 180 mV vs. Ag/AgCl are attributed to the reverse processes.

The charge passed per unit geometric area calculated for the anodic peak by integration of the current between 200 and 500 mV vs. Ag/AgCl are found to be 200 and 300 mC cm^{-2} for curves (b) and (c), respectively. No peak is visible in the case of the reference sample (curve (a)). The differences in these values indicate that only the surfaces with a 3D morphology were electrochemically active, with the deposit on SC(111) exhibiting a higher electrochemical surface area enhancement (active area/geometric area) compared to the deposit on PC. The reference sample exhibited vanishingly small charge transfer in this region due to its very low, surface area enhancement. Assuming an atomically flat monomolecular layer of $Co(OH)_2$, charge density calculation roughly gives value of 0.13 mC cm^{-2}. If the charge density passed on CoNi layer calculated from cyclic voltammogram is 300 mC cm^{-2}, than the surface enhancement of the foam layer is more then 2300 times in comparison to smooth CoNi layer.

Therefore, the morphology of the porous layer structure has a decisive influence on the kinetics of the surface redox reaction suitable as a catalyst for oxygen evolution in electrolysers. The porous CoNi layer obtained on SC(111) exhibits a superior electrochemical performance as compared to the PC deposit and to the reference sample in spite of the similarity in the structure. It is important to emphasize that the processes presented in Fig. 7b and c are reversible, and have a great potential to be used as a positive electrode in alkaline batteries.

One way to improve catalytic activity is deliberate preparation of high surface area surfaces, e.g. Pt on carbon support with a selectivity to a hydrogen oxidation and oxygen reduction reactions.[39] Still, possible higher reaction rate brought by high surface area is in great extent dependant of electrode geometry. A non-uniform microscopic porosity in the micrometer range, where the pore sizes of the electrode decrease with increasing distance from the front to the inner space, as well porosity on the nanoscale are necessary requirements to increase both, surface area and electrode activity.[34] The results presented here show high reaction rate attributed to the high area surface and good mechanical stability of the porous CoNi foam prepared on single-crystalline Cu(111).

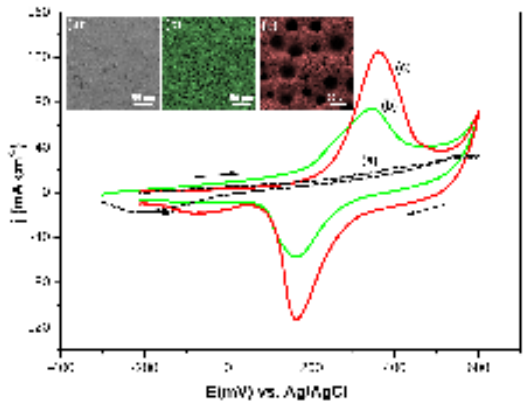

Figure 7 Cyclic voltammograms (scan rate 50 mV s^{-1}) recorded in 0.1 M KOH with electrodes made of (a) polished CoNi deposit, (b) as-grown CoNi deposit on PC Cu and (c) dendritic CoNi foam deposited on SC(111). The enhanced peaks of curve (c) are attributed to the high surface area of open foam structure. (The inserts show SEM images of the electrodes.)

4 Conclusions

CoNi layers were electrodeposited on Cu substrates with different surface structures. It is shown that morphology, microstructure, internal stress and catalytic ability of the layers are strongly influenced by the structure of the substrate.

By the use of a specially chosen single-crystalline (111) Cu substrate we achieved a uniform deposition of an open, dendritic foam structure at a relatively low current density with hydrogen bubble formation at the very beginning of the deposition. The low wettability of the single-crystalline (111) Cu substrate with low surface energy assists the adhesion of large coalescing hydrogen bubbles on the substrate. The localized flow of metal ions due to the formation of hydrogen bubbles leads to localized growth of the CoNi deposit in the form of dendrites composed of fine platelets. The resulting nanostructured CoNi alloy foam with nanosized grains shows a low level of tensile stress.

In contrast a non-porous fairly dense deposit is achieved at the same current density when using a single-crystalline (123) surface, as its increased wettability and surface energy reduce the adhesion of hydrogen bubbles. Similarly, electrodeposition on a polycrystalline Cu substrate, composed of randomly oriented grains with predominantly high surface energy. leads to a dense nanocrystalline CoNi layer.

The present approach facilitates to deposit open structures at relatively low current densities that are well attached to the surface and have a good mechanical stability. From the clearly improved results of the redox process, it can be concluded that the CoNi foam is suitable for various applications. CoNi alloy foams with high surface area have promising applications in the fields of electrocatalysis and batteries.

5 Acknowledgement

This work was supported by the Austrian Science Fund (FWF): [S10403,P22440]. Furthermore the authors acknowledge the research project "Bulk Nanostructured Materials" within the research focus "Materials Science" of the University of Vienna. The work at CEST was supported within the COMET program by the Austrian Research Promotion Agency (FFG) and the government of Lower Austria. We thank Dr. Paul Angerer for help with the X-ray measurements.

References

[1] L. Bicelli, B. Bozzini, C. Mele and L. D'Urzo, *Int. J. Electrochem. Sci*, 2008, **3**, 356–408.

[2] K. Popov, S. Djokić and B. Grgur, *Fundamental aspects of electrometallurgy*, Plenum Pub Corp, 2002.

[3] Y. Song, Y. Yang, C. Medforth, E. Pereira, A. Singh, H. Xu, Y. Jiang, C. Brinker, F. van Swol and J. Shelnutt, *J. Am. Chem. Soc*, 2004, **126**, 635–645.

[4] J. Huang, S. Vongehr, S. Tang, H. Lu, J. Shen and X. Meng, *Langmuir*, 2009, **25**, 11890–11896.

[5] J. Fang, H. Hahn, R. Krupke, F. Schramm, T. Scherer, B. Ding and X. Song, *Chem. Commun.*, 2009, 1130–1132.

[6] R. Qiu, X. Zhang, R. Qiao, Y. Li, Y. Kim and Y. Kang, *Chem. Mater*, 2007, **19**, 4174–4180.

[7] F. Jia, C. Yu, K. Deng and L. Zhang, *J. Phys. Chem. C*, 2007, **111**, 8424–8431.

[8] H. Shin, J. Dong and M. Liu, *Advanced Materials*, 2003, **15**, 1610–1614.

[9] M. Liu and L. Jiang, *Advanced Functional Materials*, 2010, **20**, 3753–3764.

[10] Y. Lai, Z. Lin, Z. Chen, J. Huang and C. Lin, *Materials Letters*, 2010, **64**, 1309–1312.

[11] A. Arico, P. Bruce, B. Scrosati, J. Tarascon and W. Van Schalkwijk, *Nature materials*, 2005, **4**, 366–377.

[12] X. Fu, Q. Xu, R. Hu, B. Pan, J. Lin and D. Liao, *Journal of power sources*, 2007, **164**, 916–920.

[13] T. Benedetti, V. Gonçales, D. Petri, S. Torresi and R. Torresi, *Journal of the Brazilian Chemical Society*, **21**, 1704–1709.

[14] H. Karnthaler, F. Prinz and G. Haslinger, *Acta Metall*, 1975, **23**, 155–163.

[15] A. Krawitz, *Introduction to diffraction in materials science and engineering*, Wiley, 2001.

[16] H. Rietveld, *Journal of Applied Crystallography*, 1969, **2**, 65–71.

[17] P. Angerer, W. Artner, E. Neubauer, L. Yu and K. Khor, *International Journal of Refractory Metals and Hard Materials*, 2008, **26**, 312–317.

[18] I. Noyan, *Springer-Verlag*, 1987.

[19] U. Welzel, J. Ligot, P. Lamparter, A. Vermeulen and E. Mittemeijer, *Journal of Applied Crystallography*, 2005, **38**, 1–29.

[20] A. Hasouna, K. Nogi and K. Ogino, *Transactions of the Japan Institute of Metals*, 1988, **29**, 812–819.

[21] D. Porter and K. Easterling, *Phase transformations in metals and alloys*, CRC, 1992.

[22] L. Rafailović, D. Minić, H. Karnthaler, J. Wosik, T. Trišović and G. Nauer, *Journal of the Electrochemical Society*, 2010, **157**, D295–D301.

[23] N. Zech, E. Podlaha and D. Landolt, *Journal of the Electrochemical Society*, 1999, **146**, 2886–2891.

[24] A. Reuss, *ZAMM-Journal of Applied Mathematics and Mechanics*, 1929, **9**, 49–58.

[25] W. Voigt, *Lehrbuch der kristallphysik*, BG Teubner, 1910.

[26] W. Martienssen and H. Warlimont, *Springer handbook of condensed matter and materials data*, Springer Verlag, 2005.

[27] A. El-Sherik, J. Shirokoff and U. Erb, *Journal of Alloys and Compounds*, 2005, **389**, 140–143.

[28] S. Hearne and J. Floro, *Journal of Applied Physics*, 2005, **97**, 14901.

[29] K. Kumar, S. Suresh, M. Chisholm, J. Horton and P. Wang, *Acta Materialia*, 2003, **51**, 387–405.

[30] D. Park, R. Song, J. Ko, B. Yoo and N. Myung, *Electrochemical and Solid-State Letters*, 2005, **8**, C23.

[31] F. Czerwinski, *Journal of the Electrochemical Society*, 1996, **143**, 3327.

[32] L. Rafailović, H. Karnthaler, T. Trisović and D. Minić, *Materials Chemistry and Physics*, 2010, **120**, 409–416.

[33] Y. Li, W. Jia and Y. Song, *Chemistry of Materials*, 2007, **19**, 5758–5764.

[34] S. Cherevko and C. Chung, *Electrochimica Acta*, 2010, **55**, 6383–6390.

[35] S. Cherevko, X. Xing and C. Chung, *Electrochemistry Communications*, 2010, **12**, 467–470.

[36] H. Shin and M. Liu, *Chemistry of materials*, 2004, **16**, 5460–5464.

[37] N. Nikolic, L. Pavlovic, M. Pavlovic and K. Popov, *Electrochimica Acta*, 2007, **52**, 8096–8104.

[38] D. Gabe, *Journal of applied Electrochemistry*, 1997, **27**, 908–915.

[39] B. Genorio, D. Strmcnik, R. Subbaraman, D. Tripkovic, G. Karapetrov, V. Stamenkovic, S. Pejovnik and N. Marković, *Nature Materials*, 2010, **9**, 998–1003.